Journal of Power Sources 269 (2014) 783–788

Contents lists available at ScienceDirect

Journal of Power Sources

journal homepage: www.elsevier.com/locate/jpowsour

Direct formic acid microfluidic fuel cell design and performance evolution

A. Moreno-Zuria [a], A. Dector [a], F.M. Cuevas-Muñiz [a], J.P. Esquivel [b], N. Sabaté [b], J. Ledesma-García [c], L.G. Arriaga [a], A.U. Chávez-Ramírez [a, *]

[a] Centro de Investigación y Desarrollo Tecnológico en Electroquímica, 76703 Querétaro, Mexico
[b] Instituto de Microelectrónica de Barcelona, IMB-CNM (CSIC), Campus UAB, 08193 Bellaterra, Barcelona, Spain
[c] División de Investigación y Posgrado, Facultad de Ingeniería, Universidad Autónoma de Querétaro, 76010 Querétaro, Mexico

HIGHLIGHTS

- The design evolution of formic acid microfluidic fuel cells is described.
- Competitive power density is reached at the lowest flow reported in a compact device.
- Stable performance is achieved for at least 30 min.
- Low cost materials and processes are used for the final DFAμFFC generation.

GRAPHICAL ABSTRACT

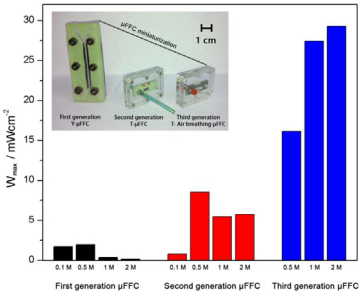

ARTICLE INFO

Article history:
Received 10 April 2014
Received in revised form
2 July 2014
Accepted 9 July 2014
Available online 17 July 2014

Keywords:
Microfluidic fuel cell evolution
Formic acid
SU-8 photoresist
Air-breathing technology
High performance

ABSTRACT

This work reports the evolution of design, fabrication and testing of direct formic acid microfluidic fuel cells (DFAμFFC), the architecture and channel dimensions are miniaturized from a thousand to few cents of micrometers. Three generations of DFAμFFCs are presented, from the initial Y-shape configuration made by a hot pressing technique; evolving into a novel miniaturized fuel cell based on microfabrication technology using SU-8 photoresist as core material; to the last air-breathing μFFC with enhanced performance and built with low cost materials and processes. The three devices were evaluated in acidic media in the presence of formic acid as fuel and oxygen/air as oxidant. Commercial Pt/C (30 wt. % E-TEK) and Pd/C XC-72 (20 wt. %, E-TEK) were used as cathode and anode electrodes respectively. The air-breathing μFFC generation, delivered up to 27.3 mW cm^{-2} for at least 30 min, which is a competitive power density value at the lowest fuel flow of 200 μL min^{-1} reported to date.

1. Introduction

In recent years, microfluidic fuel cells (μFFC) have emerged as a promising solution for small-scale power demands (e.g. laptops, cell phones, sensors and medical implants) [1–6]. μFFCs are fed by liquid fuels and oxidants under laminar flow regime; their principal goal is a longer operational time without frequent recharging [1,10]. Another important issue of these devices is that μFFCs operate without a physical barrier to separate the anode and the cathode, which implies the use of fewer components than conventional micro direct fuel cells and consequently their simplest operation and fewer maintenance events [1,11–13]. The design of μFFCs must consider the optimization of size, weight and lifetime to improve the power supply for portable devices [7–9].

* Corresponding author. Tel.: +52 442 211 6000x7842; fax: +52 442 211 6007.
E-mail address: achavez@cideteq.mx (A.U. Chávez-Ramírez).

http://dx.doi.org/10.1016/j.jpowsour.2014.07.049
0378-7753/

The use of polymeric materials like polymethyl methacrylate (PMMA) and poly-dimethylsiloxane (PDMS) has recently been proposed to construct micro-fuel cell components [8,11,12,20]. However UV-sensitive resists such as SU-8 have demonstrated to be excellent candidates to build μFFC pieces since they present some important advantages like flexibility and the capability to be sealed each other by hot-pressing technique [4,17].

In this context, three different μFFCs generations have been already developed by us in the last years with a tendency to reduce the cell size and channel dimensions [20,21]. The first μFFC generation was based in a Y-shape channel; its construction was carried out using hot-pressing technique to form the micro-channel onto a base of PMMA. In the second μFFC generation, the use of micro-fabrication technology became an important tool in order to reduce the dimensions [8,11,14–16]. The assembly consisted in a silicone polymer microchannel sandwiched between two SU-8 current collectors with a T-shape configuration. Finally, the third μFFC generation simplified the fabrication process and reduced significantly the costs by substituting of SU-8 material with a cellulose acetate film. The main modification of this generation resides on the integration of an air-exposed cathode, which enabled the oxygen admission directly from air (air-breathing). Furthermore, the 3-metal sputtering deposition was substituted by a single thin carbon film in direct contact with the catalytic material. This device that uses formic acid as fuel, is capable to achieve up to 27.3 mW cm^{-2} of maximum power density, which is a competitive power density value at the lowest flow reported to date.

2. Experimental

2.1. Construction of the three generations of μFFC

The construction of the first μFFC generation consisted on forming a microchannel by hot-press method on a PMMA base. The base was heated up to 140 °C and pressed at 24,000 lbs in^{-2} on a "Y" pattern which was previously engraved in stainless steel [1]. Current collectors consisted of a carbon Vulcan-Nafion-catalyst ink deposited on lateral faces (anode and cathode) of the PMMA channel along 45 mm (0.45 cm^2). Gold sheets were placed over the electrodes surface and a Silastic® RTV Silicone Rubber was used as gasket (see Fig. 1a). A flat plate of PMMA was used to seal the μFFC pressing at 2.5 Ncm^{-2} along the channel by screws.

The assembly in the second μFFC generation consisted in a silicone polymer microchannel sandwiched between two SU-8 current collectors (Fig. 1b). The SU-8 fabrication process was previously detailed [4], and is briefly described here. Photolithography was employed for microfabrication of the current collectors using a single layer of SU-8 50 (Microchem Corp.) on Si wafers. A sacrificial layer removed at the end of the process of releasing the SU-8 structures was used. For this step, a layer of Omnicoat TM (Microchem Corp., Newton, MA, USA) was spin-coated at 2000 rpm for 35 s followed by a baking step of 60 s at 200 °C to vaporize the solvent. Next, a layer of SU-8 50 was spin-coated at 2000 rpm for 35 s (thickness of 50 μm). The soft-bake of SU-8 layer consisted of a 60 min at 25 °C, 6 min at 65 °C, 30 min at 95 °C and 10 h cool-down at 25 °C on a hot-plate using linear ramps between temperatures. The UV-exposure was performed with an MA6/BA6 mask aligner (Karl Süss MicroTec GmbH, Garching, Germany) with a dose of 190 mJ cm^{-2} using a printed transparent foil as mask that defined the shape of the structures. Post-exposure bake consisted of 1 min at 65 °C on a hot-plate followed by 5 min at 95 °C in a convection oven. To provide electrical conductivity to SU-8 current collectors, they were covered by thin layers of Ti, Ni and Au (50 nm each one) using metal sputtering deposition (MRC-903, MRC Systems, Heidelberg, Germany). A thin film (300 μm) of silicone film was cut using a cutter plotter (Graphtec America Inc.), which was used to define the microchannel between the current collectors.

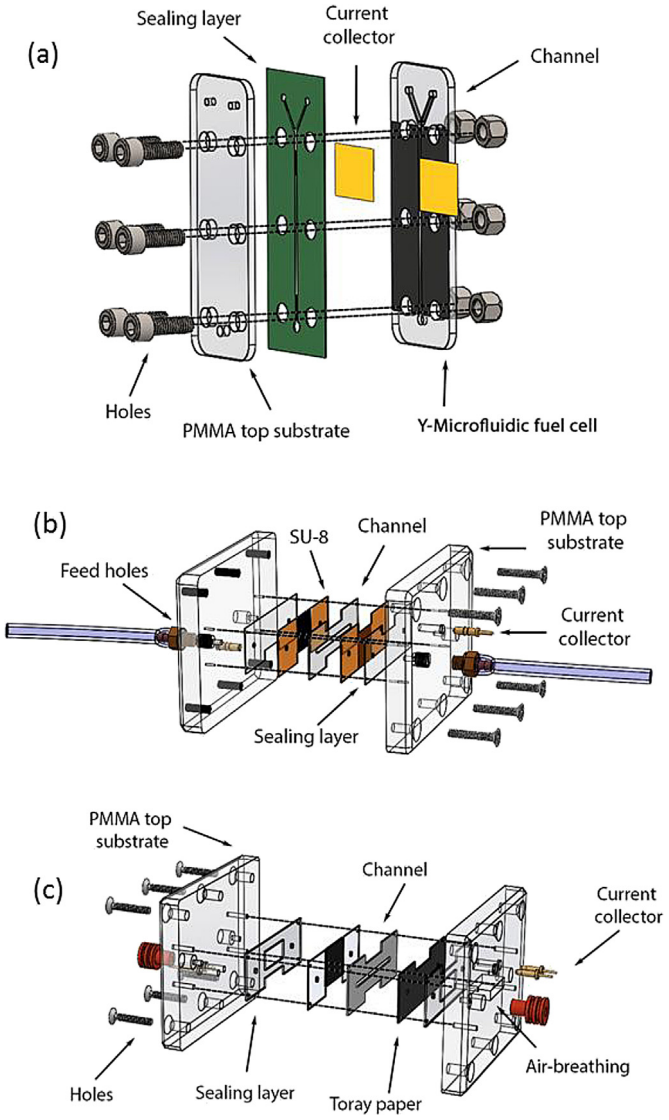

Fig. 1. Schematic representation of μFFC architecture and channel dimensions for the a) Y-shape μFFC (first generation); b) T-shape SU-8 μFFC (second generation and, c) air-breathing (third generation).

The third μFFC generation substitutes the SU-8 material in the anode for a cellulose acetate film (20 microns thick), and the same electrode shape defined by the cutter plotter above mentioned. The catalytic ink was incorporated directly over the acetate surface by homogeneous deposition using an airbrush adapted to a mini CNC (computer numerical control) system. At the cathode side, the SU-8 is substituted by Toray carbon paper (Technoquip Co Inc TGPH-120) which is covered with the catalytic material by the CNC-spray system and Au-pins are implemented for a better electrical conductivity (Fig. 1c).

Finally, the micro devices of second and third generations were sandwiched between two PMMA plates fabricated by a CNC micro milling system and tightened by screws. However, in the air-breathing type, a window on the PMMA tap is opened as an air intake and the catholyte stream consisted only of 0.5 M H_2SO_4.

Table 1
μFFC dimensions.

Generation(shape)		Length	Width	Height	Electrode active area
1st ("Y")	Cell	82 mm	30 mm	12 mm	0.45 cm^2
	Channel	20 mm	1 mm	1 mm	
2nd and 3rd ("T")	Cell	42 mm	32 mm	9.5 mm	0.09 cm^2
	Channel	20 mm	1 mm	300 μm	

2.2. Evaluation of the μFFC performance

The catalytic ink for all the μFFC generations was composed of 7 μL Nafion® 5% (Sigma–Aldrich), 73 μL isopropyl alcohol (J.T. Baker) and 1 mg electrocatalyst materials, mixed in ultrasonic bath for 20 min. The catalyst loading 1 mg cm^{-2} of Pt/C (30 wt. % E-TEK) and Pd/C XC-72 (20 wt. %, E-TEK) were maintained for cathode and anode respectively. Formic acid concentrations of 0.1, 0.5, 1 and 2 M and oxygen (4.3 U.A.P. Praxair) dissolved in 0.5 M H_2SO_4 solutions were used as fuel and oxidant aqueous solutions. The anolyte and catholyte streams were fed through the corresponding inlets in laminar flows with a Pressure-driven fluid flow from 50 to 300 μL min^{-1} using syringe pump (NE-4000, New Era Pump Systems Inc.). All tests were performed at 25 °C. Electrical measurements were performed using an Epsilon potentiostat, version 1.40.67 from Bioanalytical Systems.

3. Results and discussion

The tendency to reduce the device size and channel dimensions is shown in Table 1. Besides the dimensions, the channel geometry changed as well, a Y-shape channel was employed in the first generation (Fig. 1a); while, second and third versions used a T-shape architecture due to microfabrication challenges (Fig. 1b and c).

3.1. First μFFC generation

Polarization, power density curves and fuel flow rate characterization of this configuration have been already reported in Ref. [20]. It is worth to mention, that this cell worked only at low formic acid concentrations (0.1 and 0.5 M). At higher concentrations, the performance decreased rapidly (a limited step was reached due to low oxygen concentration). The maximum power density value reached for the first μFFC generation at 0.5 M and at 200 μL min^{-1} of HCCOH was 1.97 mW cm^{-2} with a maximum current density of 4.44 mA cm^{-2}.

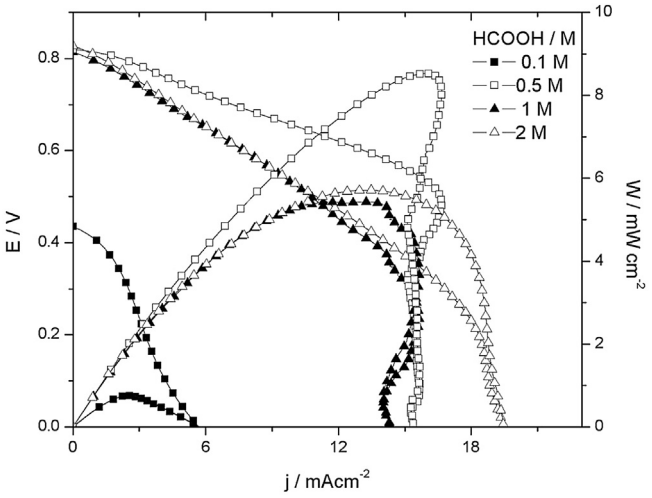

Fig. 2. SU-8 μFFC performance at several HCOOH concentrations using Pd/XC-72 and Pt/XC-72 as anode and cathode respectively.

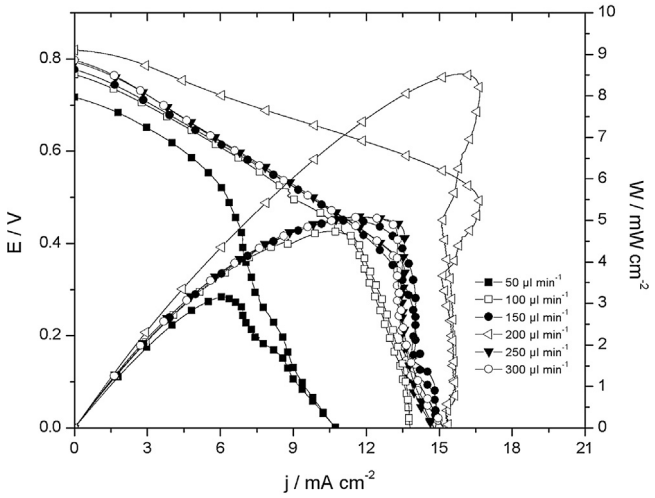

Fig. 3. μFFC second generation performance based on a fuel flow study from 50 to 300 μL min^{-1}.

3.2. Second μFFC generation (SU-8)

Fig. 2 shows the polarization and power density curves of the SU-8 generation using Pd/XC-72 as anode and Pt/XC-72 as cathode. A flow study from 50 to 300 μL min^{-1} was carried out; the best performance was identified at 200 μL min^{-1} (Fig. 3). The polarization curves recorded for this SU-8 μFFC presented the same characteristic shape of the precedent fuel cell, with well-defined regions of activation, ohmic and mass transport. At 0.5 M formic acid is interesting to note that the open circuit potential value (OCP) was similar to the previous μFFC. However, the current density values showed an important increase from 4.44 to 15.67 mA cm^{-2} to reach a maximum power density value of 8.53 mW cm^{-2} at 0.5 M formic acid (see Table 2). At higher concentrations of formic acid (1 and 2 M), the closed μFFC operation promote the formation of CO_2 bubbles blocking the channel and consequently, reducing its performance. Polarization curves were performed before and after chronoamperometric tests in order to assess the stability, Fig. 4 shows the stable performance of the SU-8 μFFC at three potential values (50 mV, 400 mV and 700 mV), as it can be observed, the μFFC was able to provide a steady current beyond 30 min Table 2 compares the performance of formic acid μFFCs reported in the literature and the SU-8 μFFC reported here; the main differences consist on the fuel concentration and the microchannel shape.

Table 2
Comparison of μFFC's performance vs. SU-8 μFFC (second generation) using formic acid and O_2 as fuel and oxidant respectively.

Reference	Electrolyte H_2SO_4 concentration	Geometry	Max power density (mW cm^{-2})
Choban et al. [14]	0.5 M	Y-shape	0.17
Cohen et al. [18]	0.1 M	F-shape	0.18
Li et al. [19]	0.1 M	F-shape	0.58
Morales-Acosta et al. [20]	0.5 M	Y-shape	3.30
Dector et al. [11]	0.5 M	Y-shape	6.70
Moreno-Zuria et al. [21]	0.5 M	T-shape	8.53

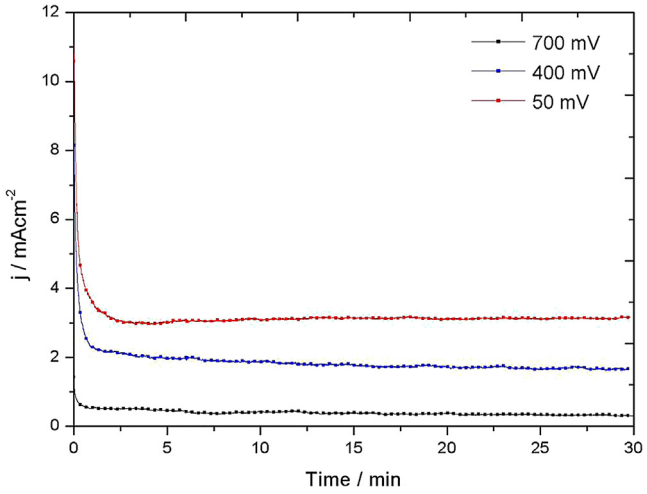

Fig. 4. Chronoamperometric curves of the SU-8 μFFC using 0.5 M HCOOH in 0.5 M H_2SO_4.

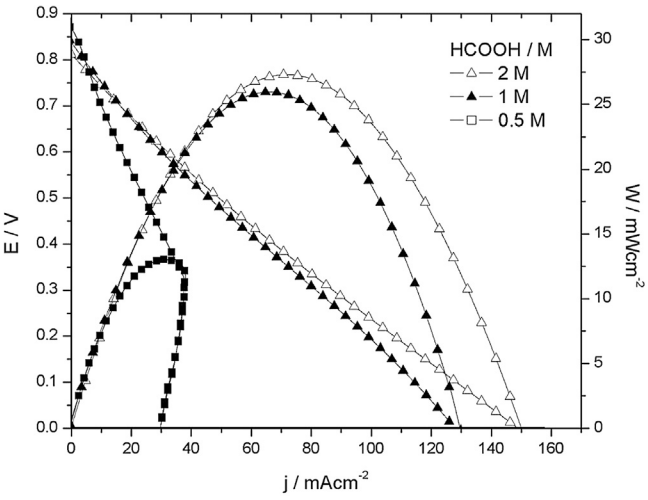

Fig. 5. Comparison of polarization and power density curves for the air-breathing μFFC using several HCOOH concentrations in 0.5 M H_2SO_4 as fuel at 25 °C under atmospheric pressure.

3.3. The compact air-breathing μFFC (third generation)

This architecture was based on the second generation μFFC, it uses the same catalyst loads but there are significant differences in materials and manufacturing techniques. Since both generations use same catalyst material for electrodes and a film of silicone for the micro-channel, the substantial cost properties resides on the core material and its preparation described in Section 2.1; cellulose acetate is widely available and it does not require any preparation before catalyst deposition, the shape is defined by a cutter plotter and no metallic deposition is required. This third generation also incorporates a window air intake and a microporous cathode described above, enhancing the oxygen availability. Since second and third generation share the same channel dimensions (length and wide, electrode separation), the optimized flow rate of 200 μl min^{-1} was fixed. Polarization and power density curves at 0.5, 1.0 and 2 M HCOOH concentration were obtained from the air-breathing μFFC and are presented in Fig. 5, on this graph can be observed that at 0.5 M, the current density reached was 30 mA cm^{-2} (two times greater than the closed μFFC) and the maximum power density was 12.95 mW cm^{-2} which represents almost twice the power of the closed μFFC. This result could be attributed to oxygen diffusivity coefficient in the air, which was higher than in solution and further to the porous characteristic of the cathode material where CO_2 produced was now released to the environment. Using a formic acid concentration of 2.0 M, the air-breathing device was able to provide up to 27.3 mW cm^{-2} and near to 152 mA cm^{-2} of maximum current density. This generation exhibited the highest performance than those displayed with first and second generation. Furthermore the maximum power density was a competitive value for μFFCs operating at low flow and taking oxygen directly from the air (not forced). Table 3 shows the μFFCs comparison in terms of fuel (formic acid and methanol), geometry, flow and structural design. Although PEMFCs present slight better performance than membraneless micro fuel cells, current membrane electrode assembly (MEA) designs are not completely adequate for miniaturized devices; complicating the development of different designs and geometries and incrementing the cost [35]. Chronoamperometric curves were carried out (Fig. 6) to observe the stability in performance and the capability to supply energy for more than 30 min.

Table 3
Comparison of air-breathing μFFC performance with similar fuel cells and methanol μFFC.

Reference	Fuel/oxidant	Flow (μL min^{-1})	Geometry	Membrane	Max power density (mW cm^{-2})
Jayashree et al. [22]	HCOOH (1 M)/air	300	F-shape	N/A	36
Zhu et al. [23]	HCOOH (1 M)/air	333	Cylinder electrodes	N/A	21.5 mW cm^{-3}
Shaeg et al. [24]	HCOOH (3 M)/air	N/A	Fuel reservoir	N/A	29
Shaeg et al. [25]	HCOOH (1 M)/air	200	T-anode porous electrode	N/A	26.5
Brushett et al. [26]	HCOOH (1 M)/air	300	F-shape	N/A	26
Hong et al. [27]	HCOOH (5 M)/air	N/A	Plate	PEM	20
Tsujiguchi et al. [28]	HCOOH (7 M)/air	200 ml min^{-1}	Plate	PEM	120
Sáez et al. [29]	HCOOH (9 M)/air	5 ml min^{-1}	Plate	PEM	13
Hollinger et al. [30]	Methanol (1 M)/pure O_2	300	T-shape	Polycarbonate separator	70
Zhong et al. [31]	Methanol (1 M)/pure O_2	400	Serpentine	Nanoporous tracketch separator at the interface	12.71
Wang et al. [32]	Methanol (6 M)/pure O_2	100 in fuel/ 20 ml min^{-1} of O_2	Serpentine	PEM	20.29
Ho Seo et al. [33]	Methanol (2 M)/air	5	Fuel storage	PEM	0.31
Jiang et al. [34]	Methanol (1 M)/air	400	N/A	PEM	2.31
Choban et al. [8]	Methanol (1 M)/ saturated O_2	300	Y-shape	N/A	12
This work (2014)	HCOOH (2 M)/air	200	T-shape	N/A	27.3

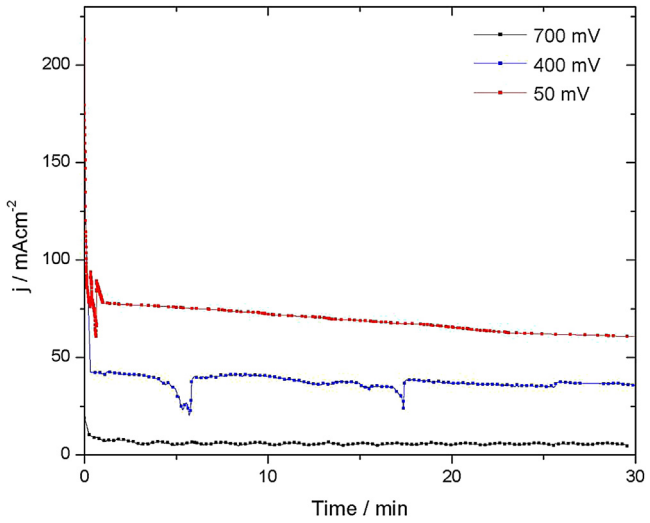

Fig. 6. Chronoamperometry of the air-breathing μFFC at 2.0 M HCOOH.

Fig. 7 compares the performance of the three μFFC generations and illustrates the miniaturization process. The μFFC evolution shows an exponential behavior in terms of power density, from few mW to tens of mW at very low fuel flow (Fig. 7A). The power delivery increases due the improvements in the core of the μFFC reflected in significant reductions in resistance values. Electrochemical impedance spectroscopy (EIS) was carried out, on this graph can be observed the difference between DFAμFFC generations in terms of impedance at open circuit voltage. In comparison between first and second generation, a significant decrease in impedance in one order of magnitude was presented (40 vs. 3 Ω cm^2 respectively), that was related to the design, fabrication materials and sealing method, decreasing the total resistance in the second generation cell. In the case of second and third generations, there was not a substantial decrease of the impedance; then, the significant increase in power density obeys mainly to the presence of the window (air breathing) that increases drastically the presence of oxygen reaching the cathode. In prospect, the size of the second and third generation dimensions can be reduced significantly by substituting the PMMA platform and incorporating novel sealing methods, which would allow the screws removal. Current collectors, connectors and tubing are as well a design challenge to overcome in order to miniaturize the whole device to a micro-scale.

4. Conclusions

The evolution of design, construction and operation of direct formic acid μFFCs is presented from the first Y-shape generation, to an optimized air-breathing μFFC. Substantial improvements on performance and dimensions were achieved based on microfabrication technology using SU-8 photoresist as core in T-shape architecture. The novel version of the μFFCs was used as a baseline to fabricate low cost μFFCs by using cheaper materials and alternative CNC systems for micromachining and catalyst spray deposition. The challenge about the limited power supply due the amount of oxygen dissolved in solution was overcome by means of incorporating an air intake over the microporous cathode. For the second and third generation excellent power density was achieved from 8.53 mW cm^{-2} to 27.3 mW cm^{-2} respectively maintaining stable performance by at least 30 min. By comparison to similar works, the air-breathing μFFC presents a competitive power density value at the lowest fuel flow reported to date, enhanced the simplified methodology employed to build a small, light and flexible direct formic acid μFFC.

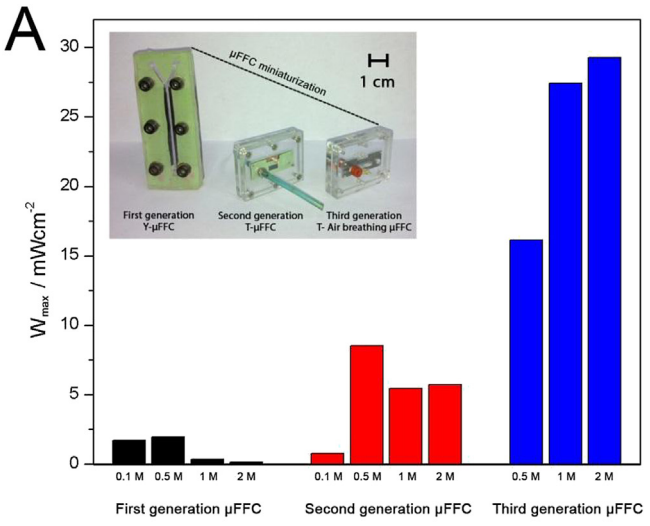

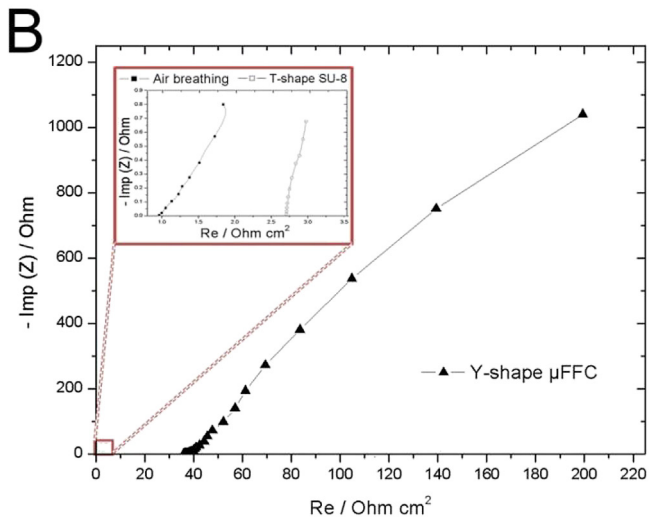

Fig. 7. Comparison of μFFC generations: (A) performance and miniaturization; (B) Electrochemical Impedance Spectroscopy at open circuit potential in a 0.5 M HCOOH.

Acknowledgments

The authors gratefully acknowledge the financial support from the Mexican Council of Science and Technology through FOMIX-QUERETARO (grant 193148) and ANR-CONACYT (grant 163114).

References

[1] E. Kjeang, N. Djilali, D. Sinton, J. Power Sources 186 (2009) 353–369.
[2] C.K. Dyer, J. Power Sources 106 (1–2) (2002) 31–34.
[3] S. Kerzenmacher, J. Ducrée, R. Zengerle, F. von Stetten, J. Power Sources 182 (2008) 1–17.
[4] J.P. Esquivel, T. Senn, P. Hernández-Fernández, J. Santander, M. Lörgen, S. Rojas, B. Löchel, C. Cané, N. Sabaté, J. Power Sources 195 (2010) 8110–8115.
[5] J.P. Esquivel, M. Castellarnau, T. Senn, B. Löchel, J. Samitier, N. Sabaté, Lab. Chip 12 (2012) 74–79.
[6] T. Ito, M. Kumimatsu, Electrochem. Commun. 8 (2006) 91–94.
[7] D. Morales-Acosta, M.D. Morales-Acosta, L.A. Godinez, L. Alvarez-Contreras, S.M. Duron-Torres, J. Ledesma-García, L.G. Arriaga, J. Power Sources 196 (2011) 9270–9275.
[8] E.R. Choban, J.S. Spendelow, L. Gancs, A. Wieckowski, P.J.A. Kenis, Electrochim. Acta 50 (2005) 5390–5398.

[9] A.S. Gago, D. Morales-Acosta, L.G. Arriaga, N. Alonso-Vante, J. Power Sources 196 (2011) 1324–1328.
[10] S.A.M. Shaegh, N.-T. Nguyen, S.H. Chan, Int. J. Hydrogen Energy 36 (2011) 5675–5694.
[11] A. Dector, J.P. Esquivel, M.J. González, M. Guerra-Balcázar, J. Ledesma-García, N. Sabaté, L.G. Arriaga, Electrochim. Acta 92 (2013) 31–35.
[12] B. Ho, E. Kjeang, Cen. Eur. J. Eng. 2 (2011) 123–131.
[13] T.M. Squires, S.R. Quake, Rev. Mod. Phys. 77 (2005) 977–1026.
[14] E.R. Choban, L.J. Markoski, A. Wieckowski, P.J.A. Kenis, J. Power Sources 128 (2004) 54–60.
[15] K. Hecker, S. Breitung, Organic and Printed Electronics, fourth ed., VDMA Verlag GmbH, Frankfurt am Main, Alemania, 2011.
[16] T. Zur Nieden, Circuit World 21 (1994) 18–27.
[17] C. Weinmueller, G. Tautschnig, N. Hotz, D. Poulikakos, J. Power Sources 195 (2010) 3849–3857.
[18] J.L. Cohen, D.A. Westly, A. Pechenik, H. Abruna, J. Power Sources 139 (2005) 96–105.
[19] A. Li, S.H. Chan, N.T. Nguyen, J. Micromech. Microeng. 17 (2007) 1107–1113.
[20] D. Morales-Acosta, G.H. Rodríguez, L.A. Godinez, L.G. Arriaga, J. Power Sources 195 (2010) 1862–1865.
[21] A. Moreno-Zuria, A. Dector, N. Arjona, M. Guerra-Balcázar, J. Ledesma-García, J.P. Esquivel, N. Sabaté, L.G. Arrriaga, A.U. Chávez-Ramírez, J. Phys. Conf. Ser. 476 (2013) 012033.
[22] R.S. Jayashree, S.K. Yoon, F.R. Brushett, P.O. Lopez-Montesinos, D. Natarajan, L.J. Markoski, P.J.A. Kenis, J. Power Sources 195 (2010) 3569–3578.
[23] X. Zhu, B. Zhang, D.-D. Ye, J. Li, Q. Liao, J. Power Sources 247 (2014) 346–353.
[24] S.A. Mousavi Shaegh, N.T. Nguyen, S.H. Chan, J. Power Sources 209 (2012) 312–317.
[25] S.A. Mousavi Shaegh, N.T. Nguyen, S.H. Chan, W. Zhou, Int. J. Hydrogen Energy 37 (2012) 3466–3476.
[26] F.R. Brushett, R.S. Jayashree, W.-P. Zhou, P.J.A. Kenis, Electrochim. Acta 54 (2009) 7099–7105.
[27] P. Hong, S. Liao, J. Zeng, X. Huang, J. Power Sources 195 (2010) 7332–7337.
[28] T. Tsujiguchi, S. Hirano, T. Iwakami, N. Nakagawa, J. Power Sources 223 (2013) 42–49.
[29] A. Sáez, E. Expósito, J. Solla-Gullón, V. Montiel, A. Aldaz, Electrochim. Acta 63 (2012) 105–111.
[30] A.S. Hollinger, R.J. Maloney, R.S. Jayashree, D. Natarajan, L.J. Markoski, P.J.A. Kenis, J. Power Sources 195 (2010) 3523–3528.
[31] L. Zhong, X. Wang, Y. Jiang, Q. Zhang, X. Qiu, Y. Zhou, L. Liu, Sens. Actuat. A-phys. 143 (2008) 70–76.
[32] X. Wang, Y. Zhu, C. Shen, Y. Zhou, X. Wu, L. Liu, Sens. Actuat. A-phys. 188 (2012) 246–254.
[33] Y. Jiang, X. Wang, L. Zhong, L. Liu, J. Micromech. Microeng. 16 (2006) 233–239.
[34] Y. Ho Seo, Y.-Ho Cho, Sens. Actuat. A-phys 150 (2009) 87–96.
[35] M.A. Goulet, E. Kjeang, J. Power Sources 260 (2014) 186–196.